Improving Robotic Tactile Localization Super-resolution via Spatiotemporal Continuity Learning and Overlapping Air Chambers

Xuyang Li[1], **Yipu Zhang**[1], **Xuemei Xie**[1, 2*], **Jiawei Li**[1], **Guangming Shi**[1, 3]

[1] Xidian University, Xi'an, 710071, China
[2] Pazhou Lab, Huangpu, 510555, China
[3] Peng Cheng Laboratory, Shenzhen, 518055, China
{xylee, ypzhang_0, jiawei_li}@stu.xidian.edu.cn, xmxie@mail.xidian.edu.cn, gmshi@xidian.edu.cn

Abstract

Human hand has amazing super-resolution ability in sensing the force and position of contact and this ability can be strengthened by practice. Inspired by this, we propose a method for robotic tactile super-resolution enhancement by learning spatiotemporal continuity of contact position and a tactile sensor composed of overlapping air chambers. Each overlapping air chamber is constructed of soft material and seals the barometer inside to mimic adapting receptors of human skin. Each barometer obtains the global receptive field of the contact surface with the pressure propagation in the hyperelastic seal overlapping air chambers. Neural networks with causal convolution are employed to resolve the pressure data sampled by barometers and to predict the contact position. The temporal consistency of spatial position contributes to the accuracy and stability of positioning. We obtain an average super-resolution (SR) factor of over 2500 with only four physical sensing nodes on the rubber surface (0.1 mm in the best case on 38×26 mm^2), which outperforms the state-of-the-art. The effect of time series length on the location prediction accuracy of causal convolution is quantitatively analyzed in this article. We show that robots can accomplish challenging tasks such as haptic trajectory following, adaptive grasping, and human-robot interaction with the tactile sensor. This research provides new insight into tactile super-resolution sensing and could be beneficial to various applications in the robotics field.

Introduction

Human skin has both high-precision force sensing and contact location super-resolution (SR) capabilities (Abraira and Ginty 2013). With tactile sensing, the human hand is able to perform delicate manipulation tasks. Remarkable progress has been made in tactile sensing while achieving fine tactile feedback for robot hands remains a major challenge. One of the main reasons is that artificial hands lack skin-comparable tactile sensors, which are flexible and stable with low complexity and high resolution. Human skin is able to perceive tactile stimulus at a spatial resolution higher than the average spacing between mechanoreceptors in the finger, for it mainly consists of four types of mechanoreceptors (SA-I, SA-II, RA-I, RA-II) (Abraira and Ginty 2013). The SA-I and SA-II refer to slow-adapting receptors and RA-I and RA-II refer to rapid-adapting receptors. The four types of adapting receptors responses are differentiated to various contact sizes and frequencies.

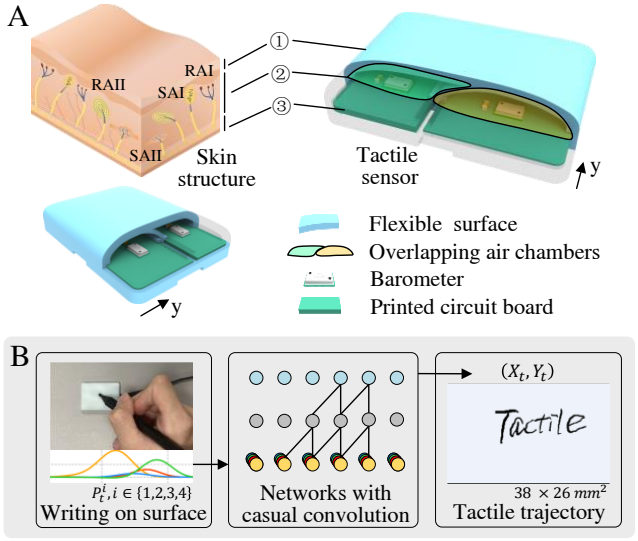

Figure 1: Illustration of the tactile sensor. A depicts the human skin structure and the soft tactile sensor with a flexible surface. B shows working principle of the tactile sensor and super-resolution localization results. The air pressure data in the four air chambers generated by the surface deformation are sent into the neural networks with causal convolution to predict the contact location. We visualized the predictions.

Tactile sensing is important for manipulators and skins of robots in unstructured environments. The tactile super-resolution with high localization accuracy is obtained by modeling the receptive fields of sensors. Based on a variety of transduction principles, many artificial tactile sensors have been proposed, including using capacitance (Lepora et al. 2015; Boutry et al. 2018; Lee et al. 2011), resistance (Park et al. 2015; Zou et al. 2018; Mu et al. 2018; Ma et al. 2015; Sun et al. 2019; Kang, Lee, and Kim 2014; Zhang et al. 2018; Kim et al. 2021), optics (Ward-Cherrier et al. 2018; Palli et al. 2014; Yuan, Dong, and Adelson 2017),

*Corresponding author.

magnetic fields (Wang et al. 2016; Ledermann et al. 2013; Tomo et al. 2018; Yan et al. 2021, 2022) and pressure (Piacenza, Sherman, and Ciocarlie 2018; Sun and Martius 2021). However, in the large body of work above, modeling tactile super-resolution localization is still done using multilayer perceptron regression instead of temporal convolution modeling.

In this paper, we present a concise and effective method for tactile localization super-resolution. Our method is to design a soft tactile sensor with four cavities and barometers embedded. In this way, each barometer achieves the global receptive field effectively with the overlapping structure. Then, we construct a tactile dataset including time series information of each physical node for the sensor and employ a network with causal convolutional modules to model the data and map the pressure distributions to contact locations on sensor surface. The structure and the working principle of the tactile sensor are shown in Figure 1. As a result, we obtain an average localization accuracy of 0.13 mm on 38×26 mm^2. According to the evaluation criteria, our method achieves the state-of-the-art tactile super-resolution factor of 2507.

There is still no very mature theory for tactile localization super-resolution, and it is generally considered to be related to the overlapping range of the receptive field of each physical node and the modeling method of the tactile sensor. To our best knowledge, our method is the first to extract the spatiotemporal continuity feature of the tactile contact position for super-resolution modeling. The change of the contact position is limited between two adjacent moments. The position of contact at the t moment should be near the contact position of the $t-1$ moment in a process of continuous contact. Method of time series modeling enriches the haptic information in the time dimension and eliminates part of the noises in the original data, thereby improving the performance of tactile localization super-resolution.

The position of the barometers in the air chambers is allowed to be changed as needed in our tactile sensor without super-resolution accuracy drops. This is different from traditional tactile super-resolution, which requires fixed physical node positions for modeling. Besides, we apply highly sensitive tactile sensory feedback in conjunction with the robotic arm to accomplish challenging tasks such as haptic trajectory following, adaptive grasping, and objects handover.

The main contributions of this paper can be summarized as follows:

- We propose a flexible tactile sensor with built-in overlapping air chambers, which brings the global receptive field for each barometer. Our tactile sensor is capable of sensing local touches on 3D surface with high accuracy.
- We employ a temporal convolution network to learn the spatiotemporal continuity of tactile contact location for the first time, which improves the accuracy and stability of tactile super-resolution.
- Our method has well generality and application potential. The position of the barometer could be adjusted as needed without super-resolution accuracy drops, while different types of soft materials and various barometers are supported.

The remainder of the article is organized as follows: in the next section, we discuss the related work from the field. In Section 3 we describe the design of the sensor and its characterization. In Section 4 we introduce the approaches for improving tactile super-resolution. Then, in Section 5, we show an evaluation of the super-resolution performance of our method in different scenarios. Finally, in Section 6, we summarize our work and give conclusions and an outlook for future research.

Related Work

Limited by the space of the robot manipulator and the integration complexity of tactile sensors, it is difficult to improve the localization accuracy of tactile perception by using a sensor array. Inspired by image super-resolution and human tactile perception mechanisms, various tactile super-resolution methods applied to different materials and sensors have also been produced. Recently, numerous transduction methodologies have been explored, and many artificial tactile sensors which have the ability of super-resolution have been proposed.

In the early period, Bayesian perception was applied to biomimetic tactile sensors which have an elastomeric covering that spreads the contact over multiple taxels. Lepora et al. (Lepora et al. 2015) achieve a 35-fold improvement of localization acuity (0.12 mm) over sensor resolution (4 mm). With the same method applied to an optical sensor, Lepora et al. (Lepora and Ward-Cherrier 2015) design the TacTip sensors, which are capable of achieving 40-fold localization super-resolution from 4 mm to 0.1 mm. Ward-Cherrier et al. (Ward-Cherrier et al. 2018) design a range of soft optical tactile sensors with various morphologies fabricated through dual-material 3D printing to attain submillimeter accuracy on a rolling cylinder task, representing greater than 10-fold super-resolved acuity. Sun and Martius (Sun and Martius 2019) make use of the spreading behavior of mechanical deformation by attaching a few strain gauges on a large robotic limb shell and developing ML methods to achieve a 78-fold super-resolution. The spreading behavior of mechanical deformation can expand the receptive field of sensors by mechanical waves in a very short time. Min Kim et al. (Kim et al. 2021) propose a supervised learning network called local message passing network (LoMP) for calibrating a piezoresistive sensor array. Through LoMP both the contact position and corresponding pressure map can be generated with a 16-fold super-resolved localization accuracy (from 5 $\times$ 5 to 20 $\times$ 20 grids).

In recent years, progress has been made in methods based on magnetism and pressure. Hellebrekers (Hellebrekers et al. 2020) design a soft magnetic skin that can estimate both the contact position (XYZ coordinates) and force magnitude. By combining the preprocessing methods for the raw magnetic field data with a neural network, Tess Hellebrekers et al. achieve a 15-fold improvement of the localization accuracy (from 15 mm to 1 mm). Yan et al. (Yan et al. 2021, 2022) design a sinusoidally magnetized flexible film, whose deformation can be detected by a Hall sensor according to

Tactile sensor type or feature	Methods of super-resolution	Improvement of localization accuracy
Soft material and optical sensors (Ward-Cherrier et al. 2018)	Transducing deformation of images	19-fold (from 4.3 to 0.22 mm)
Capacitor arrays (Lepora et al. 2015)	Bayesian perception	35-fold (from 4 to 0.12 mm)
Optical sensor (Lepora and Ward-Cherrier 2015)	Bayesian perception	40-fold (from 4 to 0.10 mm)
Pressure sensors (Piacenza, Sherman, and Ciocarlie 2018)	Machine learning	57-fold (from 68 to 1.2 mm)
Strain-gauge sensors (Sun and Martius 2019)	Machine learning	78-fold (30.8 in 24000 mm^2)
Piezoresistance sensor arrays (Kim et al. 2021)	Local message passing network	16-fold (from 25 to 400 grids)
Magnetic film (Yan et al. 2021)	Multilayer perceptron	60-fold (from 6 to 0.1 mm)
Pressure sensors (Sun and Martius 2021)	Taxel value isolines and machine learning	1254 SR factor (0.0216 in 676 mm^2, 25 sensors)
Overlapping structure and pressure sensors **(Ours)**	Causal convolution network	**2507 SR factor** (0.0983 in 988 mm^2, 4 sensors)

Table 1: Comparison of tactile super-resolution methods

the changes of magnetic flux densities under external forces. The sensor achieves a 60-fold super-resolved accuracy enhanced by multilayer perceptron (MLP). Magnetic sensors are still difficult to avoid interference from external magnetic objects. Navarroe et al. (Navarro et al. 2019) introduce a novel pneumatic mechanosensor dedicated to soft robotics and measured changes in cavity volumes inside a soft silicon pad by air-flow sensors. The average positioning accuracy is 0.6mm. In the methods of using the barometer, Piacenza et al.(Piacenza, Sherman, and Ciocarlie 2018) embed individual pressure sensors and map the raw signals from these pressure sensors to known surface locations and indentation depths with data-driven techniques. They employ machine learning (ML) to achieve a 57-fold SR. Huanbo Sun and Georg Martius (Sun and Martius 2021) propose a theory based on sensor isolines for geometric super-resolution, and link it to machine learning techniques for signal processing. Their sensors obtain an average super-resolution factor of over 100 along one-dimension (1D) and 1200 along two-dimension (2D), respectively. The super-resolution factor is calculated according to Eq. 4. For easier viewing, we list these methods in Table 1.

Sensor Design and Characterization

We construct four air chambers with overlapping structures using a soft rubber material with tear-resistant properties. As shown in Figure 2B, the four air chambers are sealed separately and overlap with each other in the three-dimensional space. Arc staggered form is employed to expand the coupling surface for pressure spreading while avoiding the excessive accumulation of materials at the connection of adjacent chambers. The gas (fluid domain) in the chambers transmits stress to the septum (solid domain) of the chambers and the septum displacement to the gas in the adjacent one. The uniform hardness of the surface is conducive to acquiring consistent pressure at each point of the sensor. The most important is that this form expands the receptive fields of the four sampling chambers, which is beneficial to the localization super-resolution.

PCBs with high-sensitivity barometers are fixed in the groove reserved in the air chamber rubber shell. We employ epoxy resin for bonding and sealing after the circuit board is embedded into the air chamber. We degassed the glue solution to ensure seal integrity, then inverted the chambers into the mold. The glue solution solidified at room temperature for 24 hours.

The scale of the sensor is 42×30 mm^2, with a level surface in the middle and a small curved surface that descends around it. Taking into account the thickness of the rubber boundary, the effective super-resolution localization area is 38×26 mm^2.

If touch or indentation occurs on any area of the surface, the contact deformation of the surface leads to changes in air pressure in one or more air chambers. At the same time, the changes of air pressure affects the load applied to the septum between chambers, thus changing its shape and the volume of the adjacent air cells. This problem is essentially a hyperelastic sealed structural analysis, considering the effect of confined air. The structure naturally reaches a stable situation with four different chambers pressure with external force and inner air pressure. The change of volume and air pressure in the chambers follows Boyle's law (West 1999).

The barometers in the four air chambers are connected to the microprocessor (ATmega328P) via the IIC bus. The air pressure data is packaged in the microprocessor after being parsed and output through the serial port. The sampling frequency is 200 Hz. The model of the barometer is MS8607, which is rated for measuring air pressure between 1 Kpa and

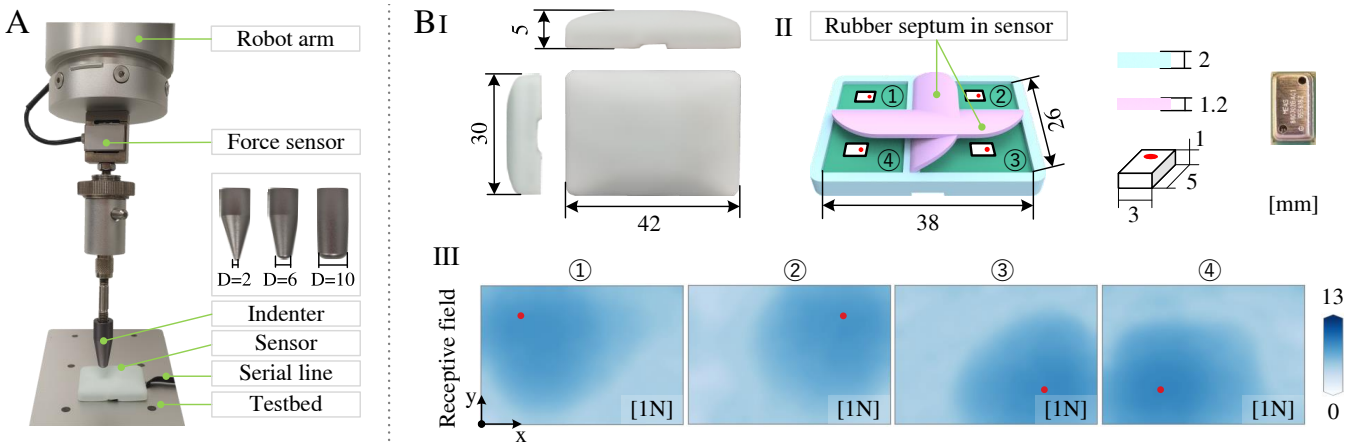

Figure 2: Illustration of the data collection system and receptive field of the sensor. A: Sensor and testbed. The program automatically records a series of time-pressure data of four sensors at one location. B: (I) is a picture of the real sensor with geometric properties on a millimeter (mm) scale. (II) shows the air chambers inside the sensor and the position of each barometer. (III) shows the global receptive field obtained by the barometer in each air chamber when a normal force of $1.0N$ is applied to a grid spaced at 0.1 mm intervals on the surface. Since the amplitude of the barometric data varies greatly, the displayed amplitude value is normalized according to the Eq. 1 and $A_t^{'x,y}|_{F=1N} = \log_2 A_t^{x,y}$. The red dot represents the location of the barometer.

200 Kpa with 2.8 Pa resolution at a 5ms response time.

Self-Labeled Data Collection Methodology

To obtain a data model of the pressure distribution of the tactile sensor, we build a self-labeled data acquisition test bench, which is shown in Figure 2A. Our test bench consists of a UR5 robotic arm and a ZNLBS-V1 force sensor with a rated range of -30N to 30N (0.05% FS repeatability, 0.1% FS non-linearity). Both the robotic arm and the force sensor are connected to a computer for real-time control and data recording via our program. Three different sizes of indenters are mounted on the end of the force sensor in turn and are moved up and down with program control. The automatic labeling program simultaneously records the time-pressure data series in the four chambers for each pressing. These time-pressure data are labeled with the pressed position (x, y) and size (ϕ) of indenter. We use a 2D plane grid of 0.1×0.1 mm^2 to project onto the sensor surface, and set the indentation depth in the Z-axis direction to a random value in the range of 0.1-2.1 mm. The sampled data are randomly divided into the training dataset and validation dataset. The training dataset consists of $90K$ groups of data while the validation dataset set is about $10K$. The details of training and testing the models at different sampling intervals of data and different shapes of indenters are discussed in detail in section 5. The collected data shows that pressing at almost any point changes the pressure in the four chambers. This indicates that the interaction effect of gas and soft material leads to the global receptive field of each barometer, which is shown in Figure 2.

Tactile Super-Resolution with Causal Convolution

Given there is a single contact with the sensor, the goal of our method is to predict the precise contact location from the changes in pressure observed. Our approach addresses the problem through spatiotemporal continuity learning with causal convolution (Oord et al. 2016) in a certain time window length. Different lengths of data sequences are generated by pressing with different forces and speeds via a fixed sampling time interval of the barometer. A sliding time window is created to sample the raw data of four channels simultaneously. These sampled data are sent to the network for training, using the same location labels. The pipeline of the network is shown in Figure 3A.

The internal air pressure is around 101 Kpa when the chambers are sealed. The range of air pressure changes caused by surface contact deformation is about $100 - 180$ Kpa. To facilitate training, we normalize the input data and ground truth (GT) with the Eq. 1 and 2, in which the μ and δ are the mean and standard deviation of all the data in the dataset. The values of x, y are $0 - 28$ mm and $0 - 36$ mm, and $bp_t^{x,y}$ represents for air pressure sampled by barometer at position x, y and time t.

$$A_t^{x,y} = \frac{(bp_t^{x,y} - \mu)}{\delta} \tag{1}$$

$$X_{GT} = \frac{x}{W}, Y_{GT} = \frac{y}{H} \tag{2}$$

The neural network resolves the contact location through the data of four channels which include the information of overlapping receptive fields. Receptive fields of different lengths in the time dimension can be obtained with a tiny causal convolution network, which is described in Eq. 3.

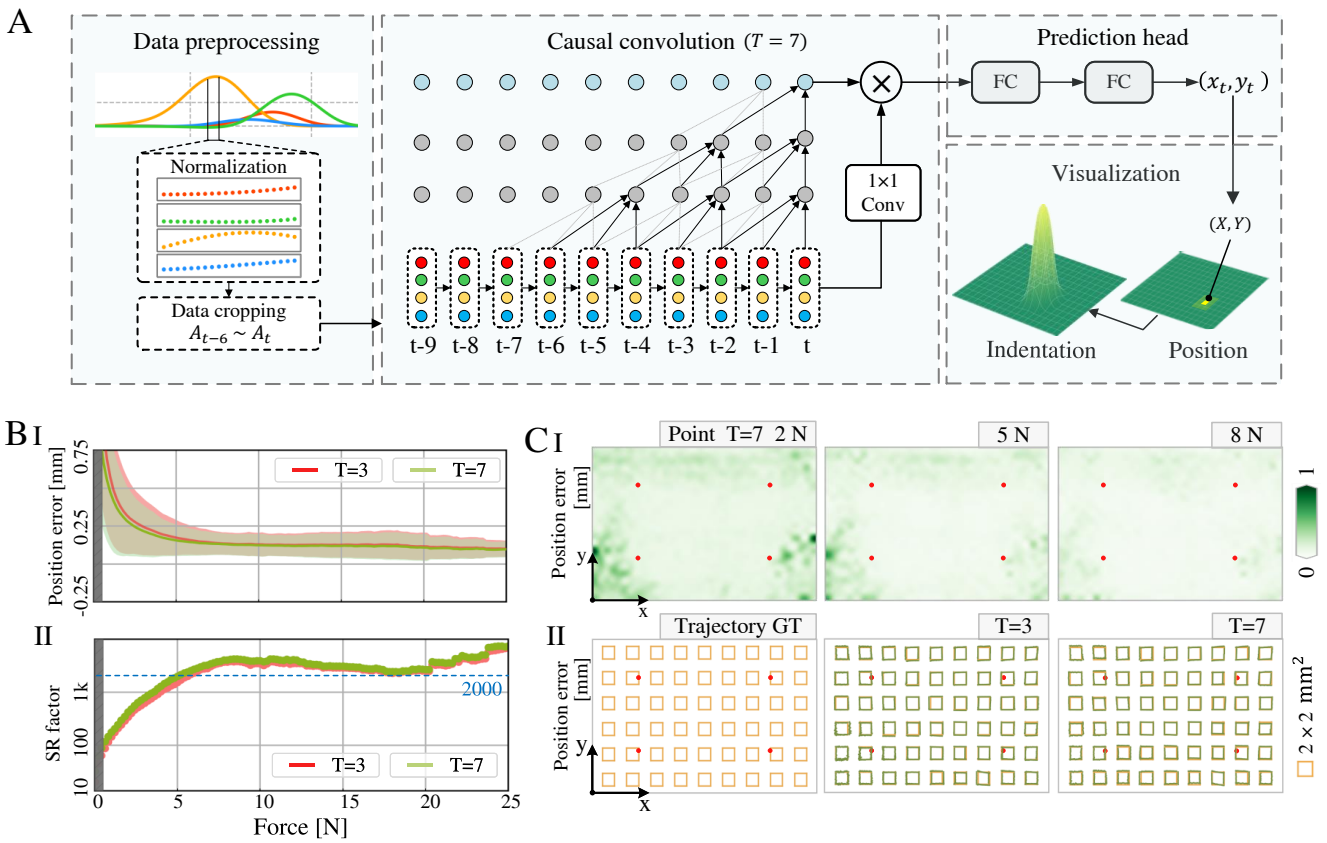

Figure 3: The pipeline of the network and experimental results of tactile super-resolution. A: Illustration of the pipeline of localization super-resolution method. The original signal is normalized by Eq. 1 and sent into the causal convolution network. The causal convolution extracts the features of the four channels signal respectively and sends the feature vectors into the multilayer perceptron. The network finally outputs the normalized predictions (x_t, y_t) and the results are visualized on the screen. B: (I) shows the mean and standard deviation of position error of estimation result of network, whose input data length is 3 and 7. (II) shows the super-resolution factor of models. C: (I) is the position error distribution corresponding to contact force magnitudes and networks with a time window of $T = 7$. (II) shows spatially resolved position error of slide trajectory in 2×2 mm^2 grids.

$$p(\mathbf{A}) = \prod_{t=1}^{T} p(A_t^{x,y} | A_1^{x,y}, ..., A_{t-1}^{x,y}) \tag{3}$$

We obtained an average super-resolution result of 0.13 mm on a soft rubber air chamber surface of 988 mm^2. This resolution exceeds the actual physical perception node by about 2507 times, which is calculated by the Eq. 4 in (Sun and Martius 2021).

$$\Omega = \frac{n_v}{n_r} = \frac{S/S_v}{n_r} \tag{4}$$

Where $S = 38{\times}26$ mm^2, and $S_v = \pi \times \sigma_{p_x} \times \sigma_{p_y}$ is the virtual taxel area calculated as an ellipse with radii of position error in x and y directions. n_v and n_r are the numbers of virtual taxels and the real sensors.

The multilayer perceptron can achieve super-resolution accuracy close to temporal convolution when the data of $T = 2$ is calculated for contact location. In the case of single-point contact, the spatial position of the sensor surface contact has the spatiotemporal continuity, and the time series information can increase the stability of position prediction.

Besides, in real scenarios, the shear force leads to the tangential deformation of the sensor surface during sliding contact. This results in a difference between the data generated by clicking and the data generated by sliding on the surface of the tactile sensor. The location information of surface contact is also associated with the time dimension. The temporal consistency of the spatial position contributes to the stability of the position estimate if the contact point does not completely leave the surface.

In causal convolution, we employ the skip connections to add low-level signal amplitude information at time t to the feature to assist in learning the contact state at the current moment. Evaluation details are discussed in next section.

Methods	MAE_x & MAE_y			
	Point		Trajectory	
MLP	0.230	0.181	0.401	0.299
Causal Conv $T = 2$	0.194	0.132	0.372	0.259
Causal Conv $T = 3$	0.187	0.123	0.369	0.241
Causal Conv $T = 4$	0.172	0.132	0.341	**0.228**
Causal Conv $T = 5$	0.169	0.129	0.330	0.236
Causal Conv $T = 6$	0.165	0.126	0.331	0.242
Causal Conv $T = 7$	0.167	0.114	0.317	0.240
Causal Conv $T = 8$	0.161	0.106	0.309	0.233
Causal Conv $T = 9$	**0.147**	**0.102**	**0.298**	**0.230**
Causal Conv $T = 10$	**0.151**	0.106	**0.299**	**0.231**
Causal Conv $T = 11$	**0.151**	**0.101**	**0.297**	**0.231**

Table 2: Results (mm) of tactile super-resolution positioning error with different time window length.

Experiments and Evaluation

The data-driven method for tactile super-resolution is straight-forward. The generalization performance of neural networks and the stability of tactile super-resolution are very important for the data-driven method. We conduct extensive experiments to verify the tactile super-resolution performance.

The temporal consistency of spatial position contributes to the stability of the tactile sensor under the influence of frictional deformation and other factors. The causal convolution models with different time window lengths and the multilayer perceptron model are trained and tested, respectively. Position prediction error of the neural network for the tactile sensor with a Shore hardness of $60A$ is shown in Table 2. Mean absolute error (MAE) and root mean square error (RMSE) are used for evaluation of prediction error.

Prediction error of single-point pressing data and trajectory data are calculated, respectively. Especially for trajectory errors, the y-axis prediction error is calculated from the trajectory in the x-axis direction, and the x-axis prediction error is calculated from the trajectory in the y-axis direction, for precise speed and location of contact are difficult to collect. The prediction errors of the trajectories are listed in Table 2. The experimental results suggest that increasing the time window length of the causal convolution can significantly improve the tactile super-resolution accuracy. The accuracy of localization super-resolution no longer increases with the consumption of neural network resource increases when the time window length $T \geq 9$. Part of the results are visualized in Figure 3C. The inference and visualization of the position are carried out on the computer. The inference time for networks from $T = 2$ to $T = 9$ is about 2.48 ms to 2.52 ms on GeForce RTX2080Ti and the parameter quantity is 0.25M to 0.40M.

We also test linear models and nonlinear regression models on this dataset, some of which are used in (Piacenza, Sherman, and Ciocarlie 2018) (Sun and Martius 2019). The results (mm) are shown in Table 3, suggesting that nonlinear models perform better on this task.

Models	LR	Ridge	DT	RF	Ours
MAE_x	6.164	6.116	0.481	0.331	**0.147**
MAE_y	3.953	3.922	0.338	0.220	**0.102**

Table 3: Localization super-resolution results (mm) of linear and nonlinear regrssion models on this dataset. The abbreviations are: 'LR' − Linear Regression, 'DT' − Decision Tree, 'RF' − Random Forest.

Accuracy Index	Sampling Intervals				
	0.1	0.2	0.5	1.0	2.0
MAE_x	**0.147**	0.180	0.199	0.202	0.306
MAE_y	**0.102**	0.117	0.139	0.173	0.285
$RMSE_x$	**0.270**	0.290	0.327	0.345	0.396
$RMSE_y$	**0.176**	0.188	0.209	0.248	0.328

Table 4: Results (mm) of causal convolution models which are trained with data of different sampling intervals.

Data Distribution and Tactile SR Accuracy

Data-driven super-resolution performance is strongly correlated with data distribution. We explore the effect of different sampling intervals of training data on the final super-resolution accuracy. The original data is sampled by dividing the two-dimensional space into small grids of 0.1×0.1 mm^2, with one press from the indenter on the robot arm in each cell. We sample at intervals of 0.2 mm, 0.5 mm, 1.0 mm, and 2.0 mm to form a subset for network training and count the average error in a 0.1×0.1 mm^2 grid on the curved sensor surface to verify the accuracy of each part. As shown in Table 4, smaller sampling intervals achieve higher localization SR accuracy.

Tactile SR Accuracy of Different Contact Size

To explore the relationship between the size of the contact point and super-resolution localization accuracy, indenters of three diameters are employed in the data collection system. The shape and size of them are shown in Figure 2A. The neural network models of different indenter diameters are trained separately and cross-tested. Similarly, the mixed dataset of three indenter diameters is used for training and testing. The mean absolute error (MAE) of them is shown in Table 5. The subsets sampled at 1mm interval on a Shore hardness of 60A sensor are used for the cross test of different indenters. The influence of the indenter diameter on the

Test Dataset	Train Dataset			
	$D = 2$	$D = 6$	$D = 10$	$Mixed$
$D = 2$	**0.174**	0.333	0.477	0.328
$D = 6$	0.361	**0.154**	0.256	**0.257**
$D = 10$	0.535	0.255	**0.169**	0.320
$Mixed$	0.268	0.221	0.308	0.267

Table 5: Results (mm) of mean error of the models trained and tested with different indenter diameters.

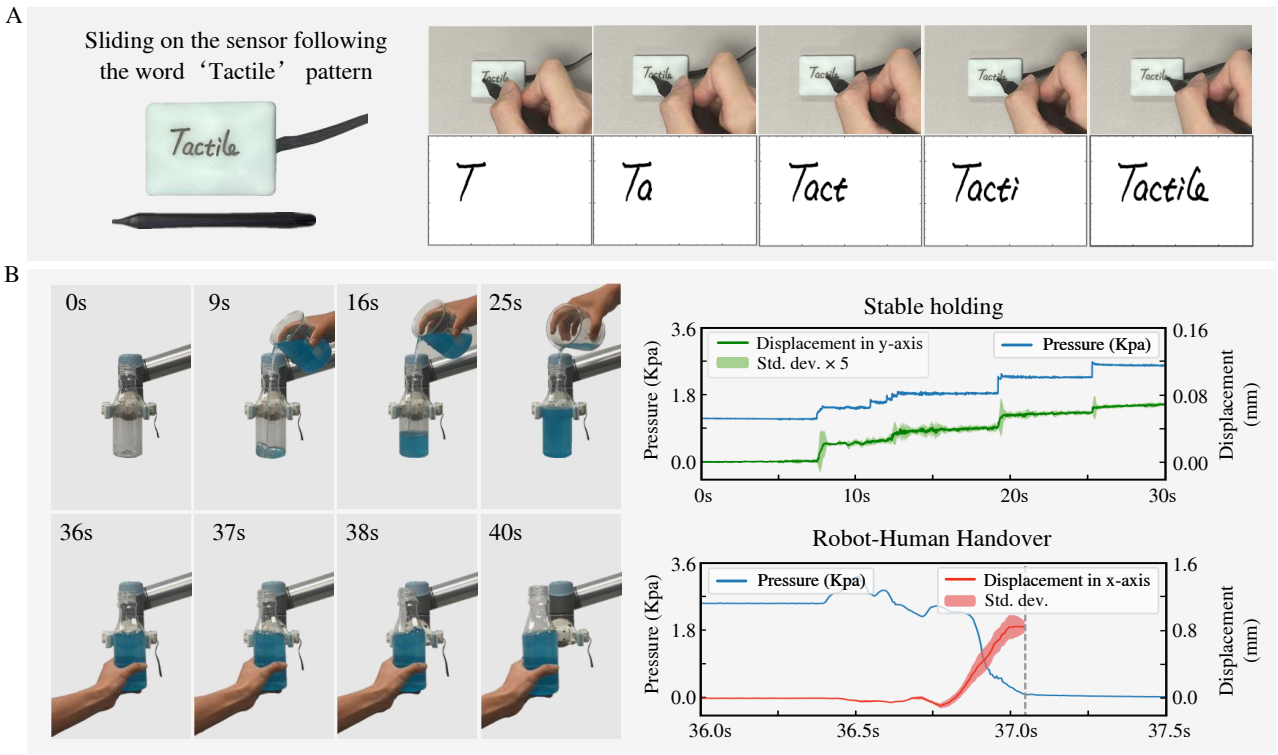

Figure 4: A: An application for super-resolution tactile sensing. A plastic pen with a 3.2 mm indenter slide on the surface following a word 'Tactile' pattern and a trained network model infers contact locations. B: An experiment of holding a bottle while filling water into it and then interacting with the human. Top: The bottle is stably held in the gripper with the slight contact deformation displacement feedback from the tactile sensor. Bottom: According to the displacement trend in different directions, the human's intention to take the bottle is detected and the gripper is released.

localization model is huge because of the variation in contact deformation. The mean error raises up to 0.6 mm. This kind of error can be reduced by training the model of mixed dataset and moderately sized indenter.

Example Applications

In this section, we describe three applications to illustrate how tactile super-resolution can benefit robot task performance. Our expectation is that it could offer far wider benefits for tactile robotics.

Many challenges remain in locating contacts in many unstructured environments or on flexible surface. Humans can even exchange intentions and information through the haptic trajectory. We use a plastic pen to write on the sensor along a fixed trajectory, and segment the trajectory according to the real-time pressure. The experimental results are shown in Figure 4A. Our sensor is extremely position sensitive. We mount the tactile sensor directly on the 3D printed gripper, which grips the empty bottle and holds it steady. At this time, the average pressure in the sensor is about 130 Kpa. As the bottle is filled with water, the vibration and slipping of the bottle are reflected in the small change of the contact position. We visualized the five times the standard deviation of the prediction position in the figure. The clamping force can be adjusted according to the value of the standard deviation and changes of contact position, so as to carry out adaptive grasping. When the bottle is full of water, the human hand takes the bottle and produces a slight displacement in the horizontal direction. The intention of human is detected according to the displacement and variance in the x-axis, the gripper is slowly released and the handover is completed. Using the tactile feedback of the sliding trend, we can well accomplish these tasks which are shown in Figure 4B.

Discussion and Future Work

In this paper, we improve robotic tactile localization super-resolution via spatiotemporal continuity learning and overlapping air chambers for the first time. We obtain an SR factor of 2507 in tactile localization accuracy with this effective method. Future work will be devoted to exploring normal force and shear force decoupling and prediction based on overlapping air chamber structures with neural networks.

Acknowledgments

This work is supported by the National Key R & D Program of China (2020AAA0109301) and National Natural Science Foundation of China (61836008).

References

Abraira, V. E.; and Ginty, D. D. 2013. The sensory neurons of touch. *Neuron*, 79(4): 618–639.

Boutry, C. M.; Negre, M.; Jorda, M.; Vardoulis, O.; Chortos, A.; Khatib, O.; and Bao, Z. 2018. A hierarchically patterned, bioinspired e-skin able to detect the direction of applied pressure for robotics. *Science Robotics*, 3(24): eaau6914.

Hellebrekers, T.; Chang, N.; Chin, K.; Ford, M. J.; Kroemer, O.; and Majidi, C. 2020. Soft magnetic tactile skin for continuous force and location estimation using neural networks. *IEEE Robotics and Automation Letters*, 5(3): 3892–3898.

Kang, M.-K.; Lee, S.; and Kim, J.-H. 2014. Shape optimization of a mechanically decoupled six-axis force/torque sensor. *Sensors and Actuators A: Physical*, 209: 41–51.

Kim, M.; Choi, H.; Cho, K.-J.; and Jo, S. 2021. Single to multi: Data-driven high resolution calibration method for piezoresistive sensor array. *IEEE Robotics and Automation Letters*, 6(3): 4970–4977.

Ledermann, C.; Wirges, S.; Oertel, D.; Mende, M.; and Woern, H. 2013. Tactile Sensor on a Magnetic Basis using novel 3D Hall sensor-First prototypes and results. In *2013 IEEE 17th International Conference on Intelligent Engineering Systems (INES)*, 55–60. IEEE.

Lee, H.-K.; Chung, J.; Chang, S.-I.; and Yoon, E. 2011. Real-time measurement of the three-axis contact force distribution using a flexible capacitive polymer tactile sensor. *Journal of Micromechanics and Microengineering*, 21(3): 035010.

Lepora, N. F.; Martinez-Hernandez, U.; Evans, M.; Natale, L.; Metta, G.; and Prescott, T. J. 2015. Tactile superresolution and biomimetic hyperacuity. *IEEE Transactions on Robotics*, 31(3): 605–618.

Lepora, N. F.; and Ward-Cherrier, B. 2015. Superresolution with an optical tactile sensor. In *2015 IEEE/RSJ International Conference on Intelligent Robots and Systems (IROS)*, 2686–2691. IEEE.

Ma, C.-W.; Hsu, L.-S.; Kuo, J.-C.; and Yang, Y.-J. 2015. A flexible tactile and shear sensing array fabricated using a novel buckypaper patterning technique. *Sensors and Actuators A: Physical*, 231: 21–27.

Mu, C.; Song, Y.; Huang, W.; Ran, A.; Sun, R.; Xie, W.; and Zhang, H. 2018. Flexible normal-tangential force sensor with opposite resistance responding for highly sensitive artificial skin. *Advanced Functional Materials*, 28(18): 1707503.

Navarro, S. E.; Goury, O.; Zheng, G.; Bieze, T. M.; and Duriez, C. 2019. Modeling novel soft mechanosensors based on air-flow measurements. *IEEE Robotics and Automation Letters*, 4(4): 4338–4345.

Oord, A. v. d.; Dieleman, S.; Zen, H.; Simonyan, K.; Vinyals, O.; Graves, A.; Kalchbrenner, N.; Senior, A.; and Kavukcuoglu, K. 2016. Wavenet: A generative model for raw audio. arXiv:1609.03499.

Palli, G.; Moriello, L.; Scarcia, U.; and Melchiorri, C. 2014. Development of an optoelectronic 6-axis force/torque sensor for robotic applications. *Sensors and Actuators A: Physical*, 220: 333–346.

Park, J.; Kim, M.; Lee, Y.; Lee, H. S.; and Ko, H. 2015. Fingertip skin–inspired microstructured ferroelectric skins discriminate static/dynamic pressure and temperature stimuli. *Science Advances*, 1(9): e1500661.

Piacenza, P.; Sherman, S.; and Ciocarlie, M. 2018. Data-driven super-resolution on a tactile dome. *IEEE Robotics and Automation Letters*, 3(3): 1434–1441.

Sun, H.; and Martius, G. 2019. Machine learning for haptics: Inferring multi-contact stimulation from sparse sensor configuration. *Frontiers in Neurorobotics*, 13: 51.

Sun, H.; and Martius, G. 2021. Theory and design of super-resolution haptic skins. arXiv:2105.11914.

Sun, X.; Sun, J.; Li, T.; Zheng, S.; Wang, C.; Tan, W.; Zhang, J.; Liu, C.; Ma, T.; Qi, Z.; et al. 2019. Flexible tactile electronic skin sensor with 3D force detection based on porous CNTs/PDMS nanocomposites. *Nano-Micro Letters*, 11(1): 1–14.

Tomo, T. P.; Regoli, M.; Schmitz, A.; Natale, L.; Kristanto, H.; Somlor, S.; Jamone, L.; Metta, G.; and Sugano, S. 2018. A new silicone structure for uSkin—A soft, distributed, digital 3-axis skin sensor and its integration on the humanoid robot iCub. *IEEE Robotics and Automation Letters*, 3(3): 2584–2591.

Wang, H.; De Boer, G.; Kow, J.; Alazmani, A.; Ghajari, M.; Hewson, R.; and Culmer, P. 2016. Design methodology for magnetic field-based soft tri-axis tactile sensors. *Sensors*, 16(9): 1356.

Ward-Cherrier, B.; Pestell, N.; Cramphorn, L.; Winstone, B.; Giannaccini, M. E.; Rossiter, J.; and Lepora, N. F. 2018. The tactip family: Soft optical tactile sensors with 3d-printed biomimetic morphologies. *Soft Robotics*, 5(2): 216–227.

West, J. B. 1999. The original presentation of Boyle's law. *Journal of Applied Physiology*, 87(4): 1543–1545.

Yan, Y.; Hu, Z.; Yang, Z.; Yuan, W.; Song, C.; Pan, J.; and Shen, Y. 2021. Soft magnetic skin for super-resolution tactile sensing with force self-decoupling. *Science Robotics*, 6(51): eabc8801.

Yan, Y.; Shen, Y.; Song, C.; and Pan, J. 2022. Tactile super-resolution model for soft magnetic skin. *IEEE Robotics and Automation Letters*, 7(2): 2589–2596.

Yuan, W.; Dong, S.; and Adelson, E. H. 2017. Gelsight: High-resolution robot tactile sensors for estimating geometry and force. *Sensors*, 17(12): 2762.

Zhang, J.; Zhou, L.; Zhang, H.; Zhao, Z.; Dong, S.; Wei, S.; Zhao, J.; Wang, Z.; Guo, B.; and Hu, P. 2018. Highly sensitive flexible three-axis tactile sensors based on the interface contact resistance of microstructured graphene. *Nanoscale*, 10(16): 7387–7395.

Zou, Z.; Zhu, C.; Li, Y.; Lei, X.; Zhang, W.; and Xiao, J. 2018. Rehealable, fully recyclable, and malleable electronic skin enabled by dynamic covalent thermoset nanocomposite. *Science Advances*, 4(2): eaaq0508.